nature neuroscience

Reorganization of cortical population activity imaged throughout long-term sensory deprivation

David J Margolis[1,2,7], Henry Lütcke[1,7], Kristina Schulz[1,2], Florent Haiss[3], Bruno Weber[2,3], Sebastian Kügler[4], Mazahir T Hasan[5,6] & Fritjof Helmchen[1,2]

Sensory maps are reshaped by experience. It is unknown how map plasticity occurs *in vivo* in functionally diverse neuronal populations because activity of the same cells has not been tracked over long time periods. Here we used repeated two-photon imaging of a genetic calcium indicator to measure whisker-evoked responsiveness of the same layer 2/3 neurons in adult mouse barrel cortex over weeks, first with whiskers intact, then during continued trimming of all but one whisker. Across the baseline period, neurons displayed heterogeneous yet stable responsiveness. During sensory deprivation, responses to trimmed whisker stimulation globally decreased, whereas responses to spared whisker stimulation increased for the least active neurons and decreased for the most active neurons. These findings suggest that recruitment of inactive, 'silent' neurons is part of a convergent redistribution of population activity underlying sensory map plasticity. Sensory-driven responsiveness is a key property controlling experience-dependent activity changes in individual neurons.

The adult brain is not hard-wired but rather must undergo plasticity to support learning and long-term adaptation to an altered environment or injury[1,2]. In response to sensory deprivation, the functional topography of the neocortex is altered such that cortical areas or 'maps' of deprived sensory inputs shrink, while maps of the remaining spared inputs expand[2,3]. Electrophysiological studies of the rodent barrel cortex, a well-characterized cortical circuit for investigating sensory processing and plasticity[4–6], have shown that layer 2/3 (L2/3) neurons are a primary locus of plasticity induced by whisker deprivation[5,6]. L2/3 neurons are the first cells in the sensory pathway to show detectable changes in firing rate and whisker tuning[7,8], and are considered one major substrate of map-level functional reorganization[9,10] (but see also ref. 11). However, it is not known how sensory-driven activity changes over time in individual L2/3 neurons and within local populations as map plasticity occurs.

A population-level description of plasticity is crucial because even neighboring neurons in rodent neocortex show a high degree of heterogeneity in their stimulus-driven spiking activity[12–15] and sensory tuning properties[14–16]. Existing studies of experience-dependent functional changes in barrel cortex have either compared neuronal activity between subjects (for example, refs. 3,5–10), or measured map-level changes in the same subject but without cellular resolution[17]. Therefore, it is not clear to what extent plasticity effects are homogeneous amongst L2/3 populations, or rather heterogeneous within subsets of neurons. Indeed, theories of map plasticity have suggested important roles for neuronal subpopulations that cannot be distinguished using classical between-subject experimental paradigms. 'Silent neurons' might be recruited during plasticity to become more active[18,19], while other cells may be expected to change in the opposite direction of the mean[20]. To test these theories, it is necessary to record activity from a large fraction of neurons in local populations—including neurons with different activity levels and tuning—and to determine the direction of functional changes over time. Activity of the same cells and populations needs to be measured repeatedly over long time periods throughout sensory deprivation as plasticity occurs, but this has not been achieved.

To address these issues, we employed chronic two-photon calcium imaging[21–23] of L2/3 neurons in the mouse barrel cortex expressing the genetically encoded calcium indicator (GECI) Yellow Cameleon 3.60 (YC3.60)[24,25]. Stable expression and functionality of YC3.60 allowed tracking sensory-evoked activity from the same individual neurons and populations over multiple weeks, before and after perturbing sensory experience by whisker trimming. While cellular responses to stimulation of the trimmed whisker were globally decreased across functional classes of neurons (defined by whisker-evoked response amplitude), responses to stimulation of the spared whisker were increased for the least active neurons and decreased for the most active neurons. Our findings highlight the power of chronic imaging to measure redistribution of activity within the same cells and populations over time during experience-dependent plasticity.

RESULTS

Chronic imaging of sensory-evoked activity using YC3.60

To longitudinally record functional responses of the exact same neurons before and after sensory deprivation, we implanted mice

[1]Brain Research Institute, University of Zurich, Zurich, Switzerland. [2]Neuroscience Center Zurich, University of Zurich and Swiss Federal Institute of Technology (ETH), Zurich, Switzerland. [3]Institute of Pharmacology and Toxicology, University of Zurich, Switzerland. [4]Center for Molecular Physiology of the Brain, University Medicine Göttingen, Department of Neurology, Göttingen, Germany. [5]Max Planck Institute for Medical Research, Heidelberg, Germany. [6]Present address: Charité – Universitätsmedizin, NeuroCure Cluster of Excellence, Berlin, Germany. [7]These authors contributed equally to this work. Correspondence should be addressed to F. Helmchen (helmchen@hifo.uzh.ch).

Received 4 May; accepted 19 September; published online 21 October 2012; doi:10.1038/nn.3240

with a cranial window[26] above the barrel cortex and performed chronic two-photon imaging[21–23] of L2/3 neurons expressing YC3.60 (refs. 24,25). Stable, dense adeno-associated virus (AAV)-mediated expression allowed us to follow the same neurons in repeated imaging sessions over several weeks (up to 161 d after AAV injection) before and after whisker trimming (**Fig. 1a** and **Supplementary Figs. 1** and **2**). Mice were anesthetized with isoflurane during imaging sessions and afterward returned to their home cages.

For standardized stimulation, we alternately deflected two neighboring whiskers, whose cortical activation areas were mapped with intrinsic optical signal (IOS) imaging (**Fig. 1b**; see Online Methods). Multiple populations were selected within the expression field close to the functional representations of both whiskers (**Fig. 1b,c**; 2–6 imaging areas per mouse; ~150 × 150 µm; median 24 neurons per population, range 11–45; **Supplementary Fig. 1**). In imaging sessions spaced days to weeks apart, we repeatedly measured whisker-evoked calcium transients (ratiometric changes $\Delta R/R$) (**Fig. 1d**) and analyzed the amplitudes of the average calcium transients per session for each of the two stimulated whiskers as a measure of response magnitude (**Fig. 1e**).

Stable functionality of YC3.60 over months

Measures of stability and plasticity of population activity critically depend on the stable functionality of the indicator itself. We first characterized YC3.60 sensitivity using simultaneous juxtacellular recordings from L2/3 neurons. Besides spontaneously occurring action potentials or burst of action potentials, whisker deflections evoked singlets or doublets (rarely three or more action potentials) (**Fig. 2a**). Action potentials elicited concomitant $\Delta R/R$ transients, the mean amplitude of which depended on the number of action potentials (**Fig. 2b**), consistent with previously reported YC3.60 sensitivity[24].

To ensure that YC3.60 reliably reports action potential-evoked calcium transients throughout the duration of our long-term experiments, we removed cranial windows >3.5 months after implantation and performed targeted juxtacellular recordings (**Fig. 2b**; $n = 3$ mice). Mean $\Delta R/R$ transients evoked by single action potentials were identical after chronic window periods (amplitude: 2.43 ± 0.25% and 2.38 ± 0.54%, decay time constant: 0.61 ± 0.04 s and 0.54 ± 0.05 s for acute and chronic, respectively; mean ± s.e.m., $P > 0.8$ for amplitude and time constant; $n = 315$ transients and 6 cells and 73 transients and 5 cells, respectively). The peak amplitudes of calcium transients evoked by electrically verified action potentials scaled similarly with the number of action potentials in acute and chronic experiments (**Fig. 2c**; regression slopes: 1.64% and 1.29% $\Delta R/R$ per action potential, respectively; $P > 0.1$).

For one neuron we could directly compare the similarity of large calcium transients after window removal and during the baseline period (**Fig. 2d**). This particular neuron also exhibited a few large burst events, for which the $\Delta R/R$ transients were well described by a summation of model single action potential-evoked transients indicating negligible indicator saturation even with large bursts (**Fig. 2e**). Furthermore, expression of individual cells remained stable over months and nuclear filled cells[23] were encountered only extremely rarely (**Supplementary Fig. 2**). We conclude that, consistent with previous optical-only measures[21,27], YC3.60 is suitable for investigating long-term changes in suprathreshold activity of individual neurons due to its high sensitivity and stable reporting of action potential firing.

Stability of responsiveness of individual neurons

Local cortical populations show remarkable heterogeneity in sensory-evoked activity[12–15], but it is not known whether the functional properties of individual barrel cortex neurons are preserved over a time scale of days and weeks[28]. In each imaging session, we measured two key functional properties of each neuron: response magnitude (mean peak $\Delta R/R$) for each of the two stimulated whiskers, and whisker tuning (preference). Note that we used mean calcium transient amplitude as a measure for response magnitude because single-trial detection rates for 1 or 2 action potentials are still below 100% for YC3.60 as well as for other GECIs[22–24,29]. Whisker tuning was defined as the relative difference in response magnitude $\Delta R/R_1$ and $\Delta R/R_2$ for the two whiskers (selectivity index, SI, ranging from −1 to +1; see Online Methods). To establish baseline properties of individual neurons in local populations, we measured the stability of response magnitude and SI in baseline sessions with whiskers intact. While most cells responded with low $\Delta R/R$, consistent with sparse firing[12–15], a small fraction of cells exhibited robust calcium transients associated with high magnitude $\Delta R/R$ responses (**Fig. 3a**). Heterogeneity of response magnitude across cells was evident in population $\Delta R/R$ plots (**Fig. 3b**). The distribution of the maximum response magnitude for either whisker ($\Delta R/R_{max}$) including 1,188 cells from 12 mice showed a consistent peak across sessions near 1% and a tail comprised of rare

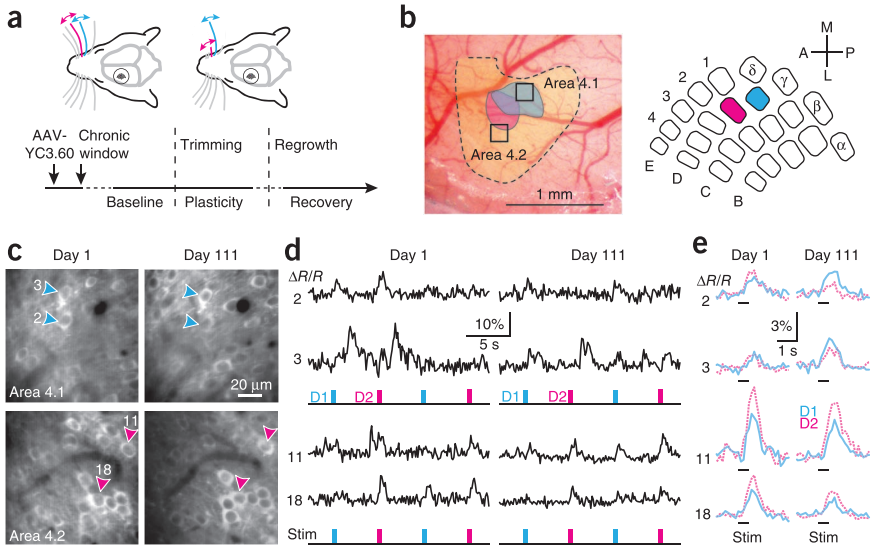

Figure 1 Long-term imaging of neuronal population activity in mouse barrel cortex. (**a**) Experimental time line. After intracortical injection of rAAV-hSYN-YC3.60 and implantation of a cranial window, mice recovered for several weeks before starting two-photon imaging sessions. Two neighboring whiskers were stimulated in repeated imaging sessions under isoflurane anesthesia spaced at least 2 d apart. Baseline (2–5 sessions), plasticity (3–9 sessions) and recovery periods (3 sessions after 12–16 weeks in two animals). (**b**) Image of cortical surface through a chronic cranial window. YC3.60 expression area shown in yellow, intrinsic signals for D1 and D2 whisker in colors (50% threshold), imaging areas indicated by squares. (**c**) Two-photon images of two L2/3 populations as marked in **b**, on an initial day and 111 d later. (**d**) Raw calcium transients ($\Delta R/R$) for two cells from each population as marked by arrowheads in **c**. Timing of whisker stimulation is indicated below traces (cyan, D1 whisker) and (magenta, D2 whisker). Areas are from mouse 4. (**e**) Averaged stimulus-evoked calcium transients ($n = 25$ per whisker) from **d**.

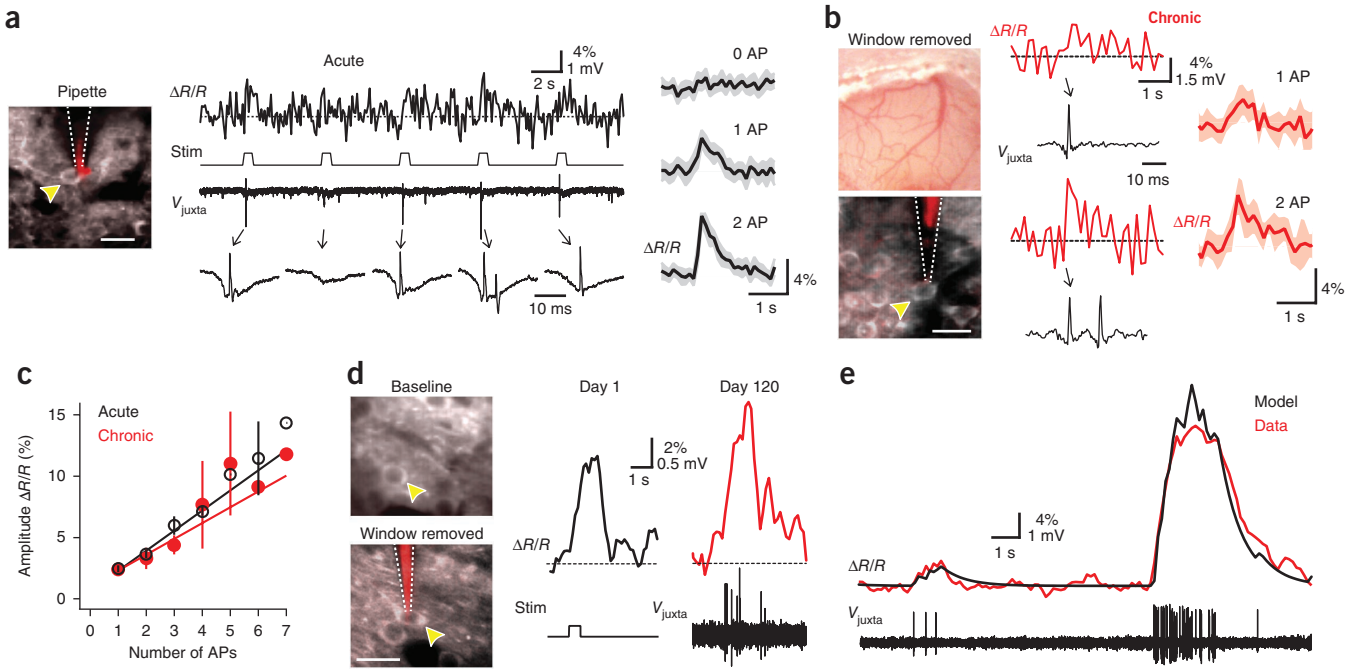

Figure 2 Long-term functionality of YC3.60. (**a**) Left: Juxtacellular recording of a YC3.60-expressing neuron in barrel cortex (arrowhead; 27 d after virus injection). Pipette containing Alexa-594 is indicated by dashed lines. Middle: Example $\Delta R/R$ trace and simultaneous voltage recording are shown for five consecutive whisker stimulations that evoked variable numbers of action potentials (AP). Right: Mean $\Delta R/R$ transients for trials exhibiting 0, 1, or 2 APs (average of 25 trials each; 95% confidence indicated). (**b**) Left: Juxtacellular voltage recording from a different L2/3 neuron (arrowhead in lower image) following removal of the cranial window 197 d after virus injection (top image). Right: Example $\Delta R/R$ transients and simultaneous voltage recordings traces evoked by 1 and 2 APs shown together with mean traces from 6 and 11 trials, respectively. (**c**) Amplitude of $\Delta R/R$ transients (mean ± s.e.m.) as a function of number of APs for acute experiments (black) and experiments after window removal (red). (**d**) Left: two-photon images of the same neuron during baseline session (41 d after virus injection, top) and after window removal (161 d, bottom). Right: Examples of $\Delta R/R$ transients from this neuron during baseline session (evoked by whisker stimulation) and after window removal with concomitant juxtacellular recording (spontaneous). (**e**) Small and large $\Delta R/R$ transients in the same neuron as in (**d**) after window removal. A model $\Delta R/R$ trace based on summation of simulated 1AP-evoked $\Delta R/R$ transients (exponential curve with amplitude and decay time constant of 1AP transients) is overlaid (black). Scale bars represent 20 µm.

high-responsive cells (**Fig. 3c**; mean difference in population $\Delta R/R$ over time, −0.01 ± 0.05, $P = 0.83$, paired t test).

Population response amplitudes were well described by a log-normal distribution on all three baseline sessions ($R^2 > 0.95$), indicating stable, sparse representations on the population level. We used this stable distribution to define three cell classes: high-responsive cells ($\Delta R/R_{max} \geq 3.6\%$ on any single baseline session, 84/1,188 cells, 7.1%), mid-responsive cells ($1.8 \leq \Delta R/R_{max} < 3.6\%$, 352 cells, 29.6%), and low-responsive cells ($\Delta R/R_{max} < 1.8\%$, 752 cells, 63.3%). Each cell class showed consistent whisker-evoked response amplitudes across sessions (**Fig. 3d**; mean $\Delta R/R$ for both whiskers). We quantified the stability of individual cell responsiveness by correlating $\Delta R/R$ values on one imaging session with $\Delta R/R$ values of the same cells on the previous session (one point per cell for each pair of sessions). We observed high correlation coefficients for both individual populations (**Fig. 3e**; $r = 0.77$, $P < 10^{-4}$) and pooled data from all cells (**Fig. 3f**; $r = 0.70$, $P < 10^{-4}$; 1,188 cells from 48 populations in 12 mice, 2,838 N versus $N + 1$ pairs). These results suggest that L2/3 neurons maintain a characteristic regime of responsiveness over days and weeks.

Flexibility of whisker tuning of individual neurons

We next investigated the persistence of baseline tuning properties. **Figure 4a** illustrates tuning of two populations in one mouse over 7 d. These populations showed opposite mean SI and peak neuropil signals (**Fig. 4b** and **Supplementary Fig. 3**), consistent with anatomical position within the barrel map (**Supplementary Fig. 4**). SI histograms for all cells (n = 1,188, 12 mice) were consistent from session to session (**Fig. 4c**) and, pooled for areas, mean population SI values showed no systematic shift over time (mean difference between sessions 0.0 ± 0.01, $P = 0.99$, paired t test) (**Fig. 4d**). In contrast, single-cell SI varied considerably in all three cell classes. 30.4% of high-responsive cells and 73.3% of low-responsive cells had opposite SI on at least one day (**Fig. 4e**), indicating that many cells did not preserve selectivity over subsequent imaging sessions. Correlation analysis of SI for all 1,188 cells between imaging sessions revealed a correlation coefficient of $r = 0.22$ ($P < 10^{-4}$; **Fig. 4f**), significantly lower than for $\Delta R/R$ (**Fig. 3e**; bootstrap t test, $P < 0.001$, 1,000 samples).

These results suggest that local populations in barrel cortex maintain stable mean tuning properties with relatively variable single neurons. There was no significant correlation between baseline SI variability (s.d.) and spatial location of neurons relative to the normalized distance to the principal barrel column ($r = 0.03$, $P = 0.25$), suggesting that variability of whisker tuning over baseline days was a common feature of neurons irrespective of position within the barrel map. Variability of individual neurons over days, although a departure from traditional views of sensory tuning, is perhaps not unexpected because L2/3 neurons possess weak whisker preference (i.e., broad receptive fields)[12,14,15], show a high baseline turnover of spines/synapses[26], and display a large potential for plasticity[2,6,7]. Indeed, simulations showed that weak whisker preference can account for the observed SI variability (**Supplementary Fig. 5**).

Map plasticity induced by whisker trimming

To investigate experience-dependent changes in barrel cortex functional organization, we trimmed all contralateral whiskers

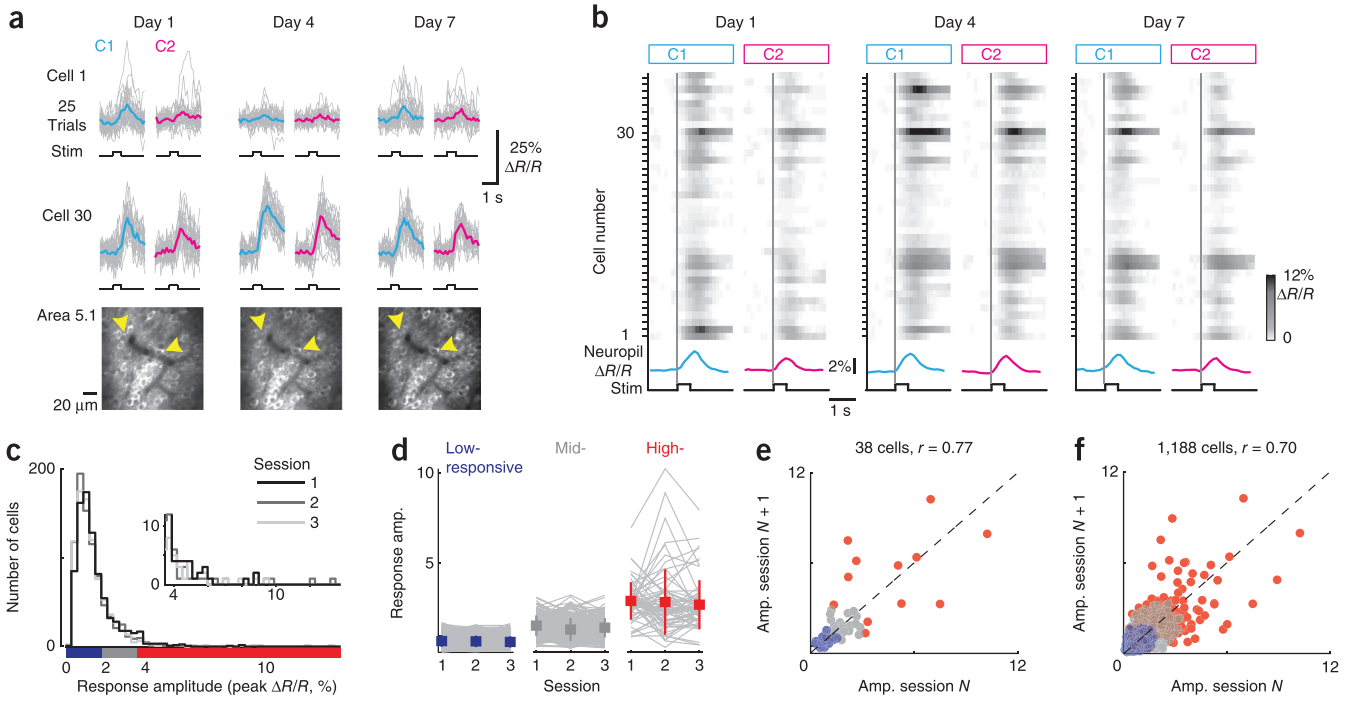

Figure 3 Stable response probabilities of cortical neurons under baseline conditions. (**a**) Example population imaged in 3 sessions over 7 d. Sensory-evoked calcium transients are shown for cells 1 and 30. Single-trial responses in gray (25 each for C1 and C2 whisker stimulation); mean in color. Stimulus (10 deflections at 20 Hz) shown below. (**b**) Mean $\Delta R/R$ plots over baseline days for the population of 38 neurons in **a**. (**c**) Distribution of $\Delta R/R_{max}$ (greater of the two whisker-evoked responses) over 3 baseline sessions for all cells ($n = 1{,}188$ in 12 mice). Mean ± s.d. for the three sessions: 1.07 ± 0.77, 0.99 ± 0.84, 0.99 ± 0.77. Color bar at bottom indicates range of $\Delta R/R_{max}$ used to define cell classes. (**d**) Mean $\Delta R/R$ (± s.e.m.) for each cell class over baseline sessions. Each group is significantly different for all between-group comparisons (all $P < 10^{-4}$, unpaired t tests) and not significantly different for between-session (within-group) comparisons (all $P > 0.5$, ANOVA). (**e**) Correlation of $\Delta R/R$ on one session with the previous session (values for each of two whiskers for each cell) for same population as in **a**. (**f**) Correlation of $\Delta R/R$ on one session with the previous session for all cells ($n = 1{,}188$ cells in 12 mice). Color code for cell classes in **e** and **f** same as in **d**.

except one (the spared whisker) of the two whiskers used for baseline stimulation, a paradigm called single whisker experience[6,8,10,30]. Whiskers were re-trimmed after each imaging session, before returning mice to their home cage, and the trimmed whisker regrew to sufficient length for stimulation by the next session (see Online Methods).

Chronic IOS imaging in the same mice used for cellular imaging (**Fig. 5a**) revealed changes in the balance between spared and trimmed whisker maps (spared-trimmed) after trimming that persisted for at least 40 d (**Fig. 5b**, top). Increases in the spared whisker map largely accounted for this effect (**Fig. 5b**, bottom). Map amplitude and area in 8/8 mice increased to favor the spared whisker (**Fig. 5c**;

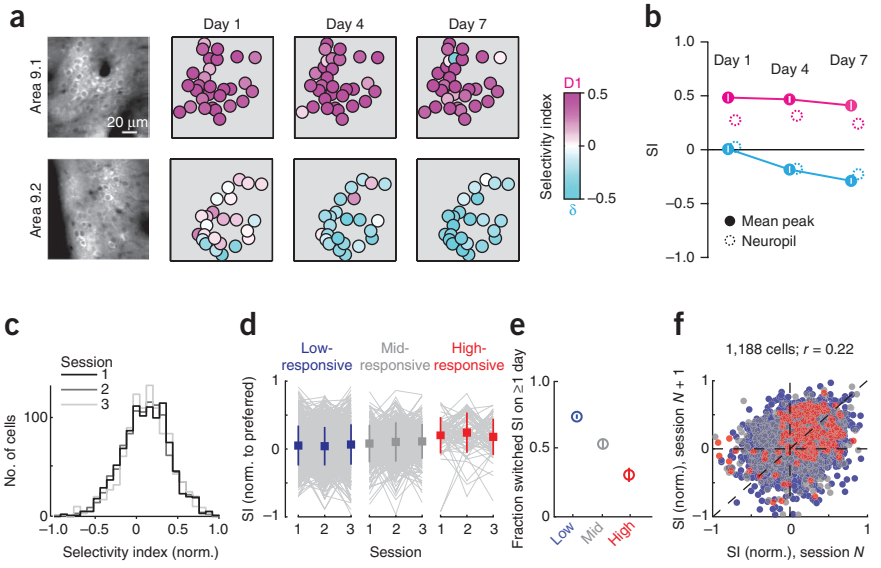

Figure 4 Flexible tuning properties over baseline days and weeks. (**a**) SI maps for two populations from the same mouse over 3 baseline imaging sessions. Magenta indicates D1 whisker preference; cyan indicates delta whisker preference. Area 9.1 was closer to the D1 column and Area 9.2 closer to the delta column. Days between imaging session indicated above. (**b**) Mean SI and frame neuropil signals over baseline imaging sessions for same populations as in **a**. (**c**) SI histograms for all cells ($n = 1{,}188$, 12 mice) overlaid for each baseline session. (**d**) Mean SI for each cell class (pooled data from 12 mice). SI is normalized to the whisker with the anatomically closer barrel column. SI values are more positive for high-responding cells, compared to the other two classes ($P < 10^{-4}$, unpaired t tests). (**e**) Fraction of cells of each cell class that switched SI on at least one baseline imaging session. (**f**) Correlation of normalized SI from one session with the previous session for all cells ($n = 1{,}188$ cells, 12 mice). Color code for cell classes in **e** and **f** same as in **d**. Error bars in **b**, **d** and **e** indicate ± s.e.m.

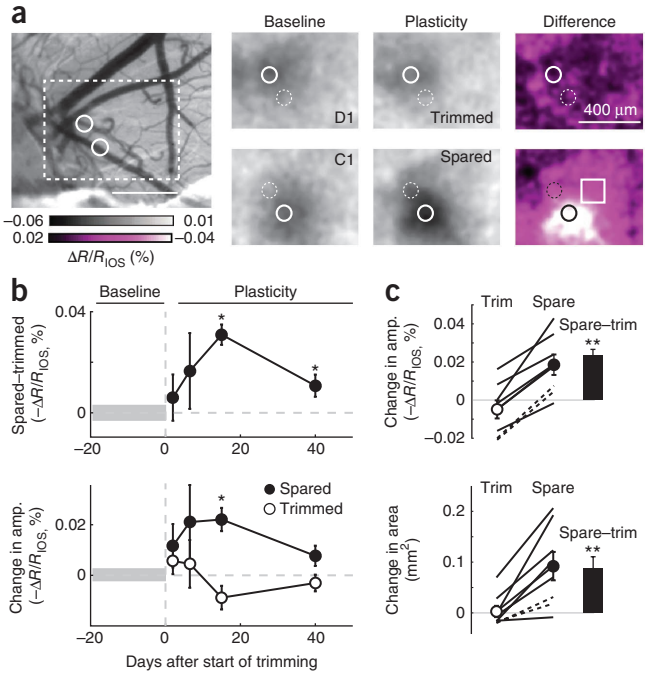

Figure 5 Map plasticity induced by whisker trimming. (**a**) Intrinsic optical signal (IOS) map expansion after whisker trimming. Left, surface blood vessels pictured 56 d after window implant (mouse 1). Circles indicate intrinsic signal locations for C1 and D1 whiskers; dashed square indicates field of view in right images. Scale bar, 400 µm. Middle, IOS averaged over 3 baseline and 3 plasticity sessions after trimming whisker D1 (6, 12, 18 d post trim). In plasticity-baseline difference image, white square indicates location of Area 1.1 in **Figure 6a**. (**b**) Time course of mean ($n = 8$ mice) change in IOS amplitude and for trimmed and spared whiskers (bottom) and the spared-trimmed difference (top). Horizontal gray line indicates s.e.m. over the baseline. Note that negative values denote increased IOS amplitude. (**c**) Mean change (plasticity-baseline) in area (bottom; relative to area at 90% peak baseline) and amplitude (top) for trimmed and spared whiskers. Lines connect data from 8 mice, including 2 mice not expressing YC3.60 (dashed lines). Error bars in **b** and **c** indicate ± s.e.m. $^*P < 0.05$, $^{**}P < 0.01$.

mean ± s.e.m. spared-trimmed difference, amplitude: 0.023 ± 0.003% $\Delta R/R_{IOS}$, $P = 10^{-4}$; area: 0.089 ± 0.002 mm^2, $P = 0.004$), including two non-YC3.60-expressing control mice (**Fig. 5c**, dotted lines). These changes corresponded to an average (± s.e.m.) 54 ± 15% increase in spared whisker map amplitude and 79 ± 38% increase in spared whisker map area (relative to area at 50% peak baseline). Consistent with previous work[5,6,17], these data indicate map expansion for the spared whisker during single whisker experience. We chose locations for cellular imaging within the spared barrel column and up to ~500 µm into the surrounding regions of cortical takeover (**Fig. 5a**, right, and **Supplementary Fig. 4**).

Neuron-specific activity changes during map plasticity

To determine how the functional properties of L2/3 neurons change during map plasticity, we repeatedly measured response magnitude and SI from the same neurons over weeks, before and after whisker trimming. In 27/29 imaging areas (n = 7 mice), neuronal populations strengthened their average selectivity for the spared whisker (**Fig. 6a**,**b**; SI baseline: −0.02 ± 0.24, SI plasticity: 0.16 ± 0.24, $P < 10^{-4}$; mean ± s.d.; paired two-tailed t test; aligned to the spared whisker; n = 734 cells, all cell classes). Time-course analysis revealed that increased selectivity for the spared whisker was detectable starting 3 d after trimming, persisted for at least 40 d, and reversed after whisker regrowth (**Fig. 6c**, all cell classes).

SI changes occurred across cell classes (mean percent ΔSI ± s.e.m.; low: 24.5 ± 1.6%, n = 434; mid: 18.9 ± 1.9%, n = 237; high: 28.7 ± 3.6%, n = 63) (**Fig. 6d**; see also **Supplementary Fig. 6**), indicating

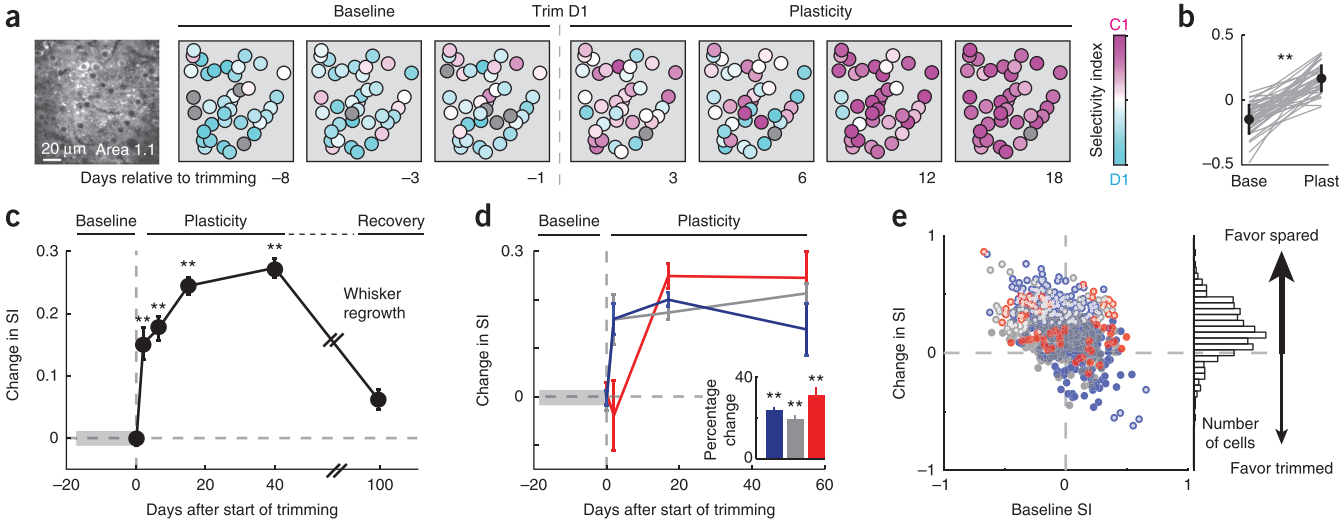

Figure 6 Retuning of neuronal selectivity. (**a**) Cellular SI maps of one population (Area 1.1) before and after D1 whisker trimming. Magenta indicates C1 whisker preference; cyan indicates D1 whisker preference. Gray cells were not identified on the respective imaging session. Days relative to trimming indicated at bottom right of frame. (**b**) Cell-wise SI changes for population in **a** (n = 38). Baseline includes 3 sessions before trimming; plasticity includes 4 sessions after trimming (mean ± s.d. baseline: −0.11 ± 0.11; plasticity: 0.25 ± 0.15; $P < 10^{-4}$, paired t test). (**c**) Time course of mean SI ± s.e.m. changes after whisker trimming (n = 29 populations, 734 cells in 7 mice). Time bins (days relative to whisker trimming): −20 to −4; −3 to 0; 1 to 3; 4 to 9; 10 to 20; 21 to 59; 60 to 120. (**d**) Time course of mean SI ± s.e.m. for each cell class. Mean percent changes (± s.e.m.; including all plasticity time points) shown in inset. (**e**) Change in SI after whisker trimming versus mean baseline SI (n = 734 cells in 7 mice). Significantly changed cells (232/734; 31.6%) indicated with white dot. Histogram at right shows change in SI for all cells (bin size 0.1). $^*P < 0.05$, $^{**}P < 0.01$.

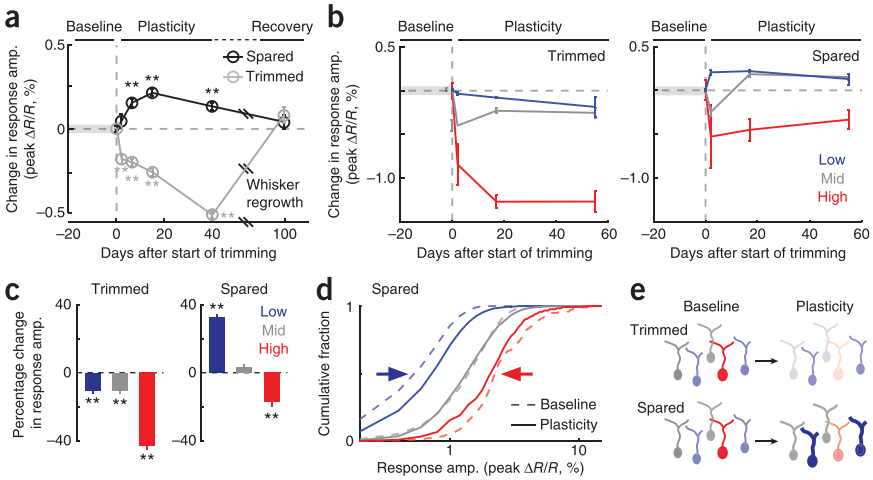

Figure 7 Differential changes in population activity depend on cell class. (**a**) Time course of mean peak $\Delta R/R$ (± s.e.m.) after whisker trimming for spared and trimmed whiskers ($n = 29$ populations, 734 cells in 7 mice). Time bins same as **Figure 6c**. (**b**) Time courses of changes in peak $\Delta R/R$ (± s.e.m.) in each cell class for trimmed (left) and spared (right) whiskers. (**c**) Mean percent changes (± s.e.m.) for each cell class. (**d**) Cumulative distributions of peak $\Delta R/R$ for each cell class before (baseline) and after (plasticity) whisker trimming. Arrows indicate the opposite changes for low- and high-responsive cells, indicating a convergent redistribution. (**e**) Cartoon of reduce and redistribute model. Changes in color saturation from baseline to plasticity indicate reduced population activity for the trimmed whisker and redistributed population activity for the spared whisker. $*P < 0.05$, $**P < 0.01$.

common retuning across low-, mid- and high-responsive cells. Neurons that initially favored the trimmed whisker tended to switch preference toward the spared whisker and neurons that initially favored the spared whisker increased their preference even further (**Fig. 6e**). Spatial analysis showed that the strongest effects were in the vicinity of the spared whisker, consistent with previous work[10] (**Supplementary Fig. 7**). Plasticity-induced changes did not depend on YC3.60 expression level (**Supplementary Fig. 8**). These results demonstrate, with cellular resolution, that map plasticity involves retuning to favor the spared whisker across cells of diverse baseline responsiveness and initial whisker preference.

We investigated whether retuning involved distinct mechanisms in different cell classes by measuring changes in the balance of responses to spared and trimmed whiskers. Overall, cells showed reduced responsiveness for the trimmed whisker (mean ± s.e.m. change in peak: -0.31 ± 0.02 $\Delta R/R$; $P < 10^{-4}$) and a smaller, delayed increase for the spared whisker (0.11 ± 0.02 $\Delta R/R$; $P < 10^{-4}$; paired t tests; $n = 734$ cells from all classes) (**Fig. 7a**). Critically, analysis of each class revealed differential shifts in the balance between $\Delta R/R_{spared}$ and $\Delta R/R_{trimmed}$ for low-, mid- and high-responsive cells. All three cell classes reduced responsiveness for the trimmed whisker over time after trimming (**Fig. 7b**, left). However, for the spared whisker, $\Delta R/R$ of low-responsive cells increased, mid-responsive cells decreased then increased, and high-responsive cells persistently decreased (**Fig. 7b**, right). Averaged over the entire time course, responsiveness for the trimmed whisker was globally reduced (mean percent change in peak $\Delta R/R_{trimmed}$ ± s.e.m.; low: $-10.5 \pm 1.5\%$, $n = 434$; mid: $-10.6 \pm 1.5\%$, $n = 237$; high: $-43.0 \pm 2.2\%$, $n = 63$), while responsiveness for the spared whisker was increased for low-responsive cells, unchanged for mid-responsive cells and reduced for high-responsive cells (mean percent change in peak $\Delta R/R_{spared}$ ± s.e.m.; low: $32.6 \pm 1.8\%$, mid: $3.4 \pm 1.5\%$, and high: $-17.3 \pm 2.9\%$) (**Fig. 7c**). These effects did not depend on exact cell class definitions, but rather showed a smooth relationship with baseline responsiveness (**Supplementary Fig. 6**). The differential changes in responsiveness across cell classes for the spared whisker represented a redistribution of population activity that converged toward the middle due to the increase for low-responsive cells and the decrease for high-responsive cells (**Fig. 7d**). Such a convergent redistribution of responsiveness for the spared whisker led to a more prominent representation of low-responsive cells and a less prominent representation of high-responsive cells within the population, as summarized in our 'reduce and redistribute' model (**Fig. 7e**) and discussed further below.

DISCUSSION

Using chronic *in vivo* imaging of a genetically encoded calcium indicator, we investigated the reorganization of neuronal population activity over weeks and months throughout cortical sensory map plasticity. We found that functionally identified low-, mid- and high-responsive L2/3 neurons displayed reliable sensory-evoked responsiveness over baseline imaging sessions spaced days apart (**Fig. 3**), supporting the proposal of stable functional cortical subnetworks involved in the coding of sensory stimuli[28,31]. After whisker trimming, responses evoked by stimulation of the trimmed whisker were reduced across low-, mid- and high-responsive cells, while responses evoked by the spared whisker were redistributed amongst them, reflecting differential retuning mechanisms in neuronal subpopulations. Highlighting the power of longitudinal imaging to reveal principles of functional reorganization, these results suggest that a fine-scale diversity of plasticity underlies the recoding of sensory stimuli within cortical microcircuits after changes in experience.

Population basis of sensory map plasticity

Sensory and motor areas of the neocortex acquire new functional properties after changes in experience, injury and learning. Such cortical plasticity has been extensively documented on the large-scale map level, but the fine-scale reorganization of activity within the underlying neuronal populations is not well understood. Previous work has reported that changes in sensory experience or behavioral training lead to a retuning of responses in deprived or untrained areas toward the spared or trained input[1–3,5,6]. How many cells retune over time, which direction they change, and how the balance of inputs controls retuning are critical issues that have only been approximated by comparing responses from different neurons and different subjects before and after plasticity has occurred. By following the same neurons longitudinally, we measured changes in tuning and sensory responsiveness from all cells in local neuronal populations, allowing a comprehensive description of the effects of experience within functionally diverse populations. Our reduce and redistribute model (**Fig. 7**) depended on the ability to measure the direction of change of the response amplitude for each whisker input in order to determine how the balance of sensory inputs caused retuning. The fraction of retuned cells that we found is larger than previously reported[8,32], probably in part because repeated measures from the same neurons are statistically more powerful than comparing across independent distributions of cells.

Critically, we found that subpopulations of neurons retuned using distinct underlying mechanisms. Low-responsive, or silent, cells

are a large pool of L2/3 neurons (roughly 60%) whose functional role in somatosensory cortex has remained mysterious[18,19]. Low-responsive cells were the only cells that on average showed increased response magnitude for the spared whisker (**Fig. 7**), supporting the hypothesis—untestable until now—that silent neurons are recruited during plasticity[18,19]. Because their activity remained below the population mean level even after trimming, it would have been impossible to distinguish silent cells without tracking response magnitude for each whisker during plasticity, as we did. This constitutes direct evidence for recruitment of silent cells as a substrate for map plasticity[18,19]. Recruitment of silent neurons might increase the overall metabolic demand of a cortical area, leading to the profound map expansion for the spared whisker as observed by IOS imaging (**Fig. 5**)[5,17]. The decrease in L2/3 cellular signals for the trimmed whisker without a clear change in IOS maps could reflect more weakly or distinctly altered responses of trimmed whisker-driven activity in L4 (refs. 7,11).

High-responsive cells retuned by a different mechanism, namely reduction of responsiveness for both the trimmed and spared whiskers (with a stronger reduction for the trimmed whisker). The reduction of responsiveness rendered high-responsive cells more similar to mid-responsive cells after plasticity. Analogous to low-responsive cells, high responders would have been difficult to distinguish from mid-responsive cells without measuring the direction of change. Because of this, it is likely that previous studies failed to distinguish high-responsive cells from the larger population because they could not detect cell-specific redistributions of activity without tracking before and after plasticity effects. High-responsive cells are likely a subset of strongly synaptically driven excitatory neurons, as suggested by other recent studies[28,31,33–35]. It is unlikely that high-responsive cells are fast-spiking (parvalbumin-positive) interneurons because of their reported counterintuitive plasticity effects[36,37] and relatively low-amplitude calcium transients[38]. Somatostatin-positive Martinotti cells are also unlikely candidates, as they hyperpolarize in response to sensory stimulation[39]. We cannot rule out the possibility that high-responders include non-fast spiking interneurons, but consider it much more likely that the majority of them are excitatory neurons, also because AAV2 tends to label excitatory neurons preferentially in cortex[35]. Taken together, our data provide evidence for differential modes of plasticity within functionally distinct neuronal subpopulations, with baseline responsiveness as a key property for determining how cells retune.

Why does responsiveness (excitability or synaptic drive) control how cells retune? It is possible that the potential for change is constrained by the cell's dynamic range. A weak synapse is more likely to potentiate than a strong synapse if the strong one is already close to the ceiling of its dynamic range. By analogy, if the same principle applies to the sensory-driven responsiveness of neurons, the dynamic range would force high responders to change selectivity by decreasing responsiveness and low responders to change by increasing responsiveness. This would result in a convergent redistribution of activity toward the middle, as we observed (**Fig. 7**). The redistribution of activity allows stimulation of the spared whisker to engage a larger fraction of neurons without a dramatic change in overall population activity. This may be a neural strategy to avoid runaway excitation, to adhere to energetic constraints, and to preserve the potential to undergo further plasticity in response to additional future events[40,41]. Together with global reduction of responses to deprived input, the redistribution of activity across cells is the first evidence for a specific population recoding strategy to optimize cortical processing capacity for salient input and could reflect increased behavioral relevance of the spared whisker[5].

Diverse cellular mechanisms underlying map plasticity

Competitive (Hebbian) synaptic interactions are thought to drive retuning in classical map plasticity, with different whisker inputs competing for control of neuronal activation: trimmed whisker input depresses and spared whisker input potentiates, leading to opposite changes in response magnitude for the trimmed and spared whiskers[2,5,6,42–44]. However, it is possible that diverse forms of plasticity are expressed within local cortical populations given that the same circuits are capable of non-Hebbian changes in alternate experimental paradigms[17] and that L2/3 neurons undergo pathway-specific forms of plasticity[20,45]. Indeed, we found a mixture of plasticity effects within cortical populations. A substantial fraction of neurons in our data set showed evidence for Hebbian-type changes, but we also found evidence for alternative mechanisms, including non-competitive (homeostatic) regulation[2,5,41,46], including the parallel up or down scaling of spared and trimmed whisker inputs (**Supplementary Fig. 6**). Homeostatic down-regulation of responsiveness for both whiskers, though still increasing selectivity for the spared whisker, was common for mid- and high-responsive cells. Thus, the balance in inputs changed distinctly across cell types of different responsiveness, supporting the idea of coexistence of diverse plasticity mechanisms within populations[5,40].

Our data suggest that diversity underlies the redistribution of responsiveness for the spared whisker in particular: Hebbian plasticity recruits low-responsive cells by strengthening their spared whisker responses, while homeostatic plasticity down regulates high-responsive cells by weakening their responses to both whiskers. Distinct synaptic mechanisms[2,30], including plasticity of inhibitory interneurons[36,37], or specific axonal rearrangements[47], could underlie these cell-specific functional changes. Future investigation of synaptic connectivity changes in anatomically or functionally defined microcircuits would help to resolve these issues. How these dynamic circuit interactions underlie the remarkable variability of baseline tuning properties of individual neurons (**Fig. 4**) is also worthy of future investigation.

Stable subnetworks for sensory coding

Our plasticity results rest upon the key observation that sparse population activity was stable over baseline days and weeks. A small fraction of highly responsive neurons (~7% of all cells) consistently occupied the tail of the response amplitude distribution (**Fig. 3**). Growing evidence indicates that the distribution of activity within cortical neuron populations is sparse[33]. Our data shows that sparse activity is stable, which allowed us to follow the trajectory of functionally defined classes of neurons throughout experience-dependent plasticity.

An essential feature of these experiments was the ultra long-term optical interrogation of neuronal activity enabled by the stable expression and functionality of YC3.60 (**Fig. 2** and **Supplementary Fig. 2**), up to 6.5 months after AAV injection. This time scale is longer than reported for other indicators[22,23,48]. YC3.60 is also more sensitive[49], allowing long-term measurement of activity from a larger fraction of the population. Although it is known that calcium buffers could potentially affect plasticity, the lack of effects of indicator expression on map plasticity (**Fig. 5**), the lack of correlation between expression level and plasticity direction (**Supplementary Fig. 8**), and the lack of effects of expression of GCaMP3 on long-term potentiation *in vitro*[48], together suggest that long-term expression of the indicator does not substantially influence the plasticity effects that we observe.

In summary, the specific plasticity effects that we found within L2/3 neuronal populations suggest a refined view of cortical plasticity that will be important for understanding the reorganization of population

activity in various neuronal circuits as it occurs naturally during myriad experience-dependent processes throughout the lifetime. Ultra long-term imaging with stable and sensitive indicators will enable longitudinal studies of cortical circuit organization related to gradual learning, forgetting, and disease progression that require investigating activity of the same neurons over several months. Chronic imaging of neuronal activity provides a powerful counterpart to structural imaging[50] and will be essential for investigations of plasticity in complete local populations, including cell types of diverse responsiveness.

METHODS

Methods and any associated references are available in the online version of the paper.

Note: Supplementary information is available in the online version of the paper.

ACKNOWLEDGMENTS

We thank H. Kasper, S. Giger and D. Göckeritz for technical assistance and A. Holtmaat, B. Gähwiler, M. Schwab, M. Thallmair and V. Planchamp for comments on an earlier version of the manuscript. This work was supported by an AMBIZIONE grant from the Swiss National Science Foundation (SNSF) to D.J.M.; a postdoctoral fellowship from the German Academic Exchange Service (DAAD) to H.L.; an SNSF grant to F. Helmchen (3100A0-114624); the EU-FP7 program (PLASTICISE project 223524 to F. Helmchen, and BRAIN-I-NETS project 243914 to F. Helmchen and F. Haiss); a grant from the Swiss SystemsX.ch initiative (project 2008/2011-Neurochoice) to F. Helmchen and B.W.; and the Max Planck Society and the Fritz Thyssen Stiftung (M.T.H.).

AUTHOR CONTRIBUTIONS

Conceived/designed the study: D.J.M., H.L., F. Helmchen; performed viral injections: D.J.M., H.L.; performed cranial window surgeries: D.J.M., F. Haiss (laboratory of B.W.); performed imaging experiments: D.J.M., H.L., K.S.; performed electrophysiology experiments: H.L., D.J.M.; produced constructs and viruses: M.T.H., S.K.; developed analysis routines: H.L.; performed analysis: H.L., D.J.M., F. Helmchen; wrote the manuscript: D.J.M., H.L., F. Helmchen.

COMPETING FINANCIAL INTERESTS

The authors declare no competing financial interests.

Published online at http://www.nature.com/doifinder/10.1038/nn.3240.
Reprints and permissions information is available online at http://www.nature.com/reprints/index.html.

1. Buonomano, D.V. & Merzenich, M.M. Cortical plasticity: from synapses to maps. *Annu. Rev. Neurosci.* **21**, 149–186 (1998).
2. Feldman, D.E. Synaptic mechanisms for plasticity in neocortex. *Annu. Rev. Neurosci.* **32**, 33–55 (2009).
3. Simons, D.J. & Land, P.W. Early experience of tactile stimulation influences organization of somatic sensory cortex. *Nature* **326**, 694–697 (1987).
4. Petersen, C.C. The functional organization of the barrel cortex. *Neuron* **56**, 339–355 (2007).
5. Feldman, D.E. & Brecht, M. Map plasticity in somatosensory cortex. *Science* **310**, 810–815 (2005).
6. Fox, K. Anatomical pathways and molecular mechanisms for plasticity in the barrel cortex. *Neuroscience* **111**, 799–814 (2002).
7. Diamond, M.E., Huang, W. & Ebner, F.F. Laminar comparison of somatosensory cortical plasticity. *Science* **265**, 1885–1888 (1994).
8. Glazewski, S. & Fox, K. Time course of experience-dependent synaptic potentiation and depression in barrel cortex of adolescent rats. *J. Neurophysiol.* **75**, 1714–1729 (1996).
9. Cheetham, C.E., Hammond, M.S., Edwards, C.E. & Finnerty, G.T. Sensory experience alters cortical connectivity and synaptic function site specifically. *J. Neurosci.* **27**, 3456–3465 (2007).
10. Glazewski, S., Chen, C.M., Silva, A. & Fox, K. Requirement for alpha-CaMKII in experience-dependent plasticity of the barrel cortex. *Science* **272**, 421–423 (1996).
11. Oberlaender, M., Ramirez, A. & Bruno, R.M. Sensory experience restructures thalamocortical axons during adulthood. *Neuron* **74**, 648–655 (2012).
12. Brecht, M., Roth, A. & Sakmann, B. Dynamic receptive fields of reconstructed pyramidal cells in layers 3 and 2 of rat somatosensory barrel cortex. *J. Physiol. (Lond.)* **553**, 243–265 (2003).
13. Crochet, S. & Petersen, C.C. Correlating whisker behavior with membrane potential in barrel cortex of awake mice. *Nat. Neurosci.* **9**, 608–610 (2006).
14. Kerr, J.N. *et al.* Spatial organization of neuronal population responses in layer 2/3 of rat barrel cortex. *J. Neurosci.* **27**, 13316–13328 (2007).
15. Sato, T.R., Gray, N.W., Mainen, Z.F. & Svoboda, K. The functional microarchitecture of the mouse barrel cortex. *PLoS Biol.* **5**, e189 (2007).
16. Rothschild, G., Nelken, I. & Mizrahi, A. Functional organization and population dynamics in the mouse primary auditory cortex. *Nat. Neurosci.* **13**, 353–360 (2010).
17. Polley, D.B., Chen-Bee, C.H. & Frostig, R.D. Two directions of plasticity in the sensory-deprived adult cortex. *Neuron* **24**, 623–637 (1999).
18. Brecht, M., Schneider, M. & Manns, I.D. Silent neurons in sensorimotor cortices: implications for plasticity. in *Neural Plasticity in Adult Somatic Sensory-Motor Systems* (ed. Ebner, F.F.), 1–19 (CRC Press, 2005).
19. Shoham, S., O'Connor, D.H. & Segev, R. How silent is the brain: is there a "dark matter" problem in neuroscience? *J. Comp. Physiol. A Neuroethol. Sens. Neural Behav. Physiol.* **192**, 777–784 (2006).
20. Jacob, V., Petreanu, L., Wright, N., Svoboda, K. & Fox, K. Regular spiking and intrinsic bursting pyramidal cells show orthogonal forms of experience-dependent plasticity in layer V of barrel cortex. *Neuron* **73**, 391–404 (2012).
21. Andermann, M.L., Kerlin, A.M. & Reid, R.C. Chronic cellular imaging of mouse visual cortex during operant behavior and passive viewing. *Front Cell Neurosci* **4**, 3 (2010).
22. Mank, M., *et al.* A genetically encoded calcium indicator for chronic in vivo two-photon imaging. *Nat. Methods* **5**, 805–811 (2008).
23. Tian, L. *et al.* Imaging neural activity in worms, flies and mice with improved GCaMP calcium indicators. *Nat. Methods* **6**, 875–881 (2009).
24. Lütcke, H. *et al.* Optical recording of neuronal activity with a genetically-encoded calcium indicator in anesthetized and freely moving mice. *Front Neural Circuits* **4**, 9 (2010).
25. Nagai, T., Yamada, S., Tominaga, T., Ichikawa, M. & Miyawaki, A. Expanded dynamic range of fluorescent indicators for Ca(2+) by circularly permuted yellow fluorescent proteins. *Proc. Natl. Acad. Sci. USA* **101**, 10554–10559 (2004).
26. Holtmaat, A. *et al.* Long-term, high-resolution imaging in the mouse neocortex through a chronic cranial window. *Nat. Protoc.* **4**, 1128–1144 (2009).
27. Minderer, M. *et al.* Chronic imaging of cortical sensory map dynamics using a genetically encoded calcium indicator. *J. Physiol. (Lond.)* **590**, 99–107 (2012).
28. Yassin, L. *et al.* An embedded subnetwork of highly active neurons in the neocortex. *Neuron* **68**, 1043–1050 (2010).
29. Wallace, D.J. *et al.* Single-spike detection in vitro and in vivo with a genetic Ca2+ sensor. *Nat. Methods* **5**, 797–804 (2008).
30. Clem, R.L., Celikel, T. & Barth, A.L. Ongoing in vivo experience triggers synaptic metaplasticity in the neocortex. *Science* **319**, 101–104 (2008).
31. Lefort, S., Tomm, C., Floyd Sarria, J.C. & Petersen, C.C. The excitatory neuronal network of the C2 barrel column in mouse primary somatosensory cortex. *Neuron* **61**, 301–316 (2009).
32. Glazewski, S., Giese, K.P., Silva, A. & Fox, K. The role of alpha-CaMKII autophosphorylation in neocortical experience-dependent plasticity. *Nat. Neurosci.* **3**, 911–918 (2000).
33. Barth, A.L. & Poulet, J.F. Experimental evidence for sparse firing in the neocortex. *Trends Neurosci.* **35**, 345–355 (2012).
34. Crochet, S., Poulet, J.F., Kremer, Y. & Petersen, C.C. Synaptic mechanisms underlying sparse coding of active touch. *Neuron* **69**, 1160–1175 (2011).
35. O'Connor, D.H., Peron, S.P., Huber, D. & Svoboda, K. Neural activity in barrel cortex underlying vibrissa-based object localization in mice. *Neuron* **67**, 1048–1061 (2010).
36. Yazaki-Sugiyama, Y., Kang, S., Cateau, H., Fukai, T. & Hensch, T.K. Bidirectional plasticity in fast-spiking GABA circuits by visual experience. *Nature* **462**, 218–221 (2009).
37. Gandhi, S.P., Yanagawa, Y. & Stryker, M.P. Delayed plasticity of inhibitory neurons in developing visual cortex. *Proc. Natl. Acad. Sci. USA* **105**, 16797–16802 (2008).
38. Hofer, S.B. *et al.* Differential connectivity and response dynamics of excitatory and inhibitory neurons in visual cortex. *Nat. Neurosci.* **14**, 1045–1052 (2011).
39. Gentet, L.J. *et al.* Unique functional properties of somatostatin-expressing GABAergic neurons in mouse barrel cortex. *Nat. Neurosci.* **15**, 607–612 (2012).
40. Nelson, S.B. & Turrigiano, G.G. Strength through diversity. *Neuron* **60**, 477–482 (2008).
41. Turrigiano, G.G. & Nelson, S.B. Hebb and homeostasis in neuronal plasticity. *Curr. Opin. Neurobiol.* **10**, 358–364 (2000).
42. Diamond, M.E., Armstrong-James, M. & Ebner, F.F. Experience-dependent plasticity in adult rat barrel cortex. *Proc. Natl. Acad. Sci. USA* **90**, 2082–2086 (1993).
43. Celikel, T., Szostak, V.A. & Feldman, D.E. Modulation of spike timing by sensory deprivation during induction of cortical map plasticity. *Nat. Neurosci.* **7**, 534–541 (2004).
44. Hebb, D.O. *The Organization of Behavior: A Neuropsychological Theory* (Wiley, New York, 1949).
45. Wen, J.A. & Barth, A.L. Input-specific critical periods for experience-dependent plasticity in layer 2/3 pyramidal neurons. *J. Neurosci.* **31**, 4456–4465 (2011).
46. Mrsic-Flogel, T.D. *et al.* Homeostatic regulation of eye-specific responses in visual cortex during ocular dominance plasticity. *Neuron* **54**, 961–972 (2007).
47. Cheetham, C.E., Hammond, M.S., McFarlane, R. & Finnerty, G.T. Altered sensory experience induces targeted rewiring of local excitatory connections in mature neocortex. *J. Neurosci.* **28**, 9249–9260 (2008).
48. Huber, D. *et al.* Multiple dynamic representations in the motor cortex during sensorimotor learning. *Nature* **484**, 473–478 (2012).
49. Yamada, Y. *et al.* Quantitative comparison of genetically encoded Ca indicators in cortical pyramidal cells and cerebellar Purkinje cells. *Front Cell Neurosci* **5**, 18 (2011).
50. Hübener, M. & Bonhoeffer, T. Searching for engrams. *Neuron* **67**, 363–371 (2010).

ONLINE METHODS

Animal preparation. Experimental procedures followed the guidelines of the Veterinary Office of Switzerland and were approved by the Cantonal Veterinary Office in Zurich. Mice (C57BL/6J, male or female, 32–45 d old, 16 mice in total) were anesthetized with ketamine (80 mg per kilogram body weight) plus xylazine (10–16 mg/kg; intraperitoneal injection), or isoflurane (4% induction, 1% maintenance). About 100 nl of recombinant adeno-associated virus 1/2 hybrid serotype vector containing YC3.60 under control of the human synapsin promoter[24] was stereotaxically injected into the whisker-related somatosensory cortex (~250 µm depth). Infectious virus titer was 3×10^8 transducing units per µl as determined in primary neuron cultures. To facilitate intraparenchymal administration we diluted 1:1 with 20% hypertonic D-mannitol solution[51]. Chronic cranial windows and head-posts were implanted 4–7 weeks following virus injection according to published procedures[26]. Briefly, mice were re-anaesthetized with isoflurane (4% induction, 1% maintenance) and a 3–4 mm craniotomy was performed at the injection site. A cover class (square 3-mm side length or round 4-mm diameter) was placed directly onto the exposed dura mater and sealed to the skull using dental cement. An aluminum head-post (<1 g) was secured to the skull with dental cement. Chronic two-photon imaging commenced earliest 14 d after window implantation. In 7 mice whisker trimming was performed after 1–2 weeks baseline imaging and imaging was continued up to 17 weeks thereafter. In 5 additional mice repeated imaging was performed over 1–6 weeks baseline periods (**Supplementary Fig. 1**).

Whisker stimulation and trimming protocol. For each imaging session, mice were anesthetized with isoflurane (4% induction, 0.5–1% maintenance). Constant ~1 Hz breathing rate was ensured, within and across sessions, using a pressure sensor under the chest and adjusting isoflurane levels accordingly. We alternately stimulated two neighboring whiskers using custom-built piezo-stimulators (20 Hz square-wave pulses for 0.5 s; 5.12 s inter-stimulus interval). Each whisker was inserted under visual control using a stereoscope to a distance of 2 mm from the whisker pad into a metal rod (from a 20-gauge needle) glued to a piezoelectric bending element. About 500 µm caudal-rostral deflections were evoked (~14° amplitude). 20–25 stimulation trials were performed per whisker, imaging area and session in order to maximize the number of regions imaged per mouse and to avoid overloading trimmed whiskers with sensory input. To verify that the correct whiskers were stimulated and that consistent locations of cortex were activated, we used intrinsic optical signal (IOS) imaging after each session.

Trimming of all contralateral whiskers but one was performed immediately or a few days after the last baseline session by cutting whiskers to fur level (<1mm). Ipsilateral whiskers were not trimmed. Subsequently, whiskers were re-trimmed after each imaging session. Trimmed whiskers regrew to sufficient length for stimulation by the next imaging session. Mice were returned to their standard home cages after each imaging session (1–4 mice per cage; 12/12 h light cycle). In a control experiment, similar cellular responses and IOS maps were elicited with trimmed and normal-length whiskers, indicating effective stimulation independent of length as reported previously[10,52,53]. In 2 animals we let whiskers re-grow for several weeks after measuring plasticity effects and performed two or three further imaging sessions to study recovery.

Functional mapping and selection of imaging areas. Virus injections resulted in ~1–2 mm diameter expression areas covering several barrel columns and infecting > 50% of L2/3 neurons[24]. In initial screening sessions under isoflurane anesthesia (0.5–1%), we selected 2–6 imaging areas per mouse for two-photon imaging. Area selection was based on density of neuronal labeling, choosing clearly discernible local populations (11–45 neurons), and lack of imaging obstructions by blood vessels. Area positions were defined relative to two barrel columns identified by functional mapping using IOS imaging[54]. Briefly, we illuminated the cortical surface with 630 nm LED light, stimulated single whiskers (2–4° rostro-caudal deflections at 10 Hz), and collected reflectance images through a 4× objective with a CCD camera (Toshiba TELI CS3960DCL; 12-bit; 3-pixel binning, 427 × 347 binned pixels, 8.6 µm pixel size, 10 Hz frame rate). Intrinsic signal changes were computed as fractional changes in reflectance relative to the pre-stimulus average (50 frames; expressed as $\Delta R/R_{IOS}$). Locations of barrel column centers for stimulated whiskers were determined by averaging intrinsic signals (8–20 trials), median filtering (5 pixel radius), and thresholding to find signal minima. Reference surface vasculature images were obtained using 546 nm LED illumination. IOS imaging was performed after chronic two-photon imaging sessions with piezo-stimulators in the same positions as during cellular imaging. Intrinsic signals were registered across days to the blood vessel pattern (TurboReg; http://bigwww.epfl.ch/thevenaz/turboreg/), averaged, background subtracted and Gaussian filtered (s.d. of 2 pixel radius). Changes in area were defined as the change relative to the area at 90% peak of the averaged baseline signal. IOS magnitude was measured as the minimum peak amplitude of the averaged filtered image.

Repeated two-photon calcium imaging. We used a custom-built two-photon microscope, equipped with a Ti:sapphire laser system (~100 fs laser pulses; Millenia X and Tsunami; Newport Spectra Physics), a custom prechirping unit, galvanometric scan mirrors (model 6210; Cambridge Technology), and a Pockels cell (Conoptics) for laser intensity modulation. For ratiometric measurements we excited YC3.60 at 870 nm and simultaneously collected CFP and YFP fluorescence through a blue (450–475 nm) and green (535–550 nm) emission filter, respectively (AHF Analysentechnik, Tübingen). Two-photon images (128 × 128 pixel; 140–150 µm imaging fields) were acquired at 7.81 Hz using a water-immersion objective (40 × LUMPlanFl/IR, 0.8 NA; Olympus). Data acquisition was controlled with software custom-written in LabVIEW (National Instruments). Imaging areas were re-found using blood vessels and local YC3.60 expression pattern as landmarks. A fixed position of the animal holder ensured consistent orientation of focal planes across sessions. YC3.60 signals were recorded in 4-5 60 s long frame scan episodes per imaging area in each session.

Electrophysiology. In 3 mice we removed the cranial window 16–19 weeks after implantation and performed targeted juxtacellular recordings from YC3.60-expressing L2/3 neurons. Neurons were visually targeted by two-photon imaging with glass pipettes (5–7 MΩ) containing Ringer solution (in mM: 135 NaCl, 5.4 KCl, 5 HEPES, 1.8 $CaCl_2$; 1 $MgCl_2$, pH 7.2 with NaOH; plus 0.025 mM Alexa-594 for pipette visualization[24]). Action potentials were recorded in current-clamp mode using an Axoclamp 2-B amplifier (Axon Instruments, Molecular Devices) and digitized using custom LabVIEW-software. Amplitude and decay time constant of action potential–related YC3.60 calcium signals were determined as described[24]. Data from the window-removal experiments were compared with data from four additional mice in acute *in vivo* experiments without previous chronic window preparations.

Data analysis. Image analysis was performed in Matlab (Mathworks) and ImageJ (NIH). Cellular regions of interest (ROI) were determined semi-automatically, using active contour based image segmentation[55]. YC3.60 is a FRET indicator that reports calcium with a decrease in CFP and increase in YFP fluorescence. We calculated the ratiometric calcium signal for each ROI as

$$R = \frac{F_{YFP}}{F_{CFP}} \quad (1)$$

$$\frac{\Delta R}{R} = \frac{R - R_0}{R_0} \quad (2)$$

where F_{YFP} and F_{CFP} refer to background-subtracted ROI fluorescence. Baseline ratio R_0 was dynamically computed in 10-frame pre-stimulus periods. Whisker selectivity was defined as the relative difference in response magnitude $\Delta R/R_1$ and $\Delta R/R_2$ for the two whiskers,

$$SI = \frac{\frac{\Delta R}{R_1} - \frac{\Delta R}{R_2}}{\frac{\Delta R}{R_1} + \frac{\Delta R}{R_2}} \quad (3)$$

For baseline analysis (except for the example of **Fig. 4a**,**b**), SI values were normalized, meaning that $\Delta R/R_1$ refers to the whisker with its barrel column anatomically closer to the imaging area (SI > 0 for selectivity toward closer barrel column). For plasticity analysis SI was calculated so that positive values indicate spared whisker preference. To determine significance of individual cells' SI changes following whisker trimming (**Fig. 6e**), we adopted a local pooled error strategy frequently employed in microarray studies[56]. Briefly, the variance in selectivity for each neuron across baseline and plasticity sessions was adjusted by taking

into account the distribution of variances versus selectivity for the population of cells (individually for each area). We calculated the smoothed variance for each cell by determining the adjusted variance based on a linear fit to variance – SI distribution

$$\sigma^2_{\text{pooled}} = \frac{\sigma^2_{\text{base}}(\text{Med}_{\text{base}})}{n_{\text{base}}} + \frac{\sigma^2_{\text{trim}}(\text{Med}_{\text{trim}})}{n_{\text{trim}}} \quad (4)$$

where $\sigma^2(\text{Med})$ is the variance associated with the observed median SI and n the number of replicates for pre- and post-trimming sessions, respectively. The local pooled error statistic[56] can be calculated as

$$z = \frac{\text{Med}_{\text{trim}} - \text{Med}_{\text{base}}}{\sigma_{\text{pooled}}} \quad (5)$$

and follows a z-distribution.

Statistical analysis. Data are presented as ± s.e.m. unless otherwise stated. Paired or unpaired two-tailed *t* tests were used to test significance, as indicated throughout the text. Significance was measured at the level of $P < 0.05$.

51. Mastakov, M.Y., Baer, K., Xu, R., Fitzsimons, H. & During, M.J. Combined injection of rAAV with mannitol enhances gene expression in the rat brain. *Mol. Ther.* **3**, 225–232 (2001).
52. Drew, P.J. & Feldman, D.E. Intrinsic signal imaging of deprivation-induced contraction of whisker representations in rat somatosensory cortex. *Cereb. Cortex* **19**, 331–348 (2009).
53. Foeller, E., Celikel, T. & Feldman, D.E. Inhibitory sharpening of receptive fields contributes to whisker map plasticity in rat somatosensory cortex. *J. Neurophysiol.* **94**, 4387–4400 (2005).
54. Chen-Bee, C.H. *et al.* Visualizing and quantifying evoked cortical activity assessed with intrinsic signal imaging. *J. Neurosci. Methods* **97**, 157–173 (2000).
55. Li, B. & Acton, S.T. Active contour external force using vector field convolution for image segmentation. *IEEE Trans. Image Process.* **16**, 2096–2106 (2007).
56. Jain, N. *et al.* Local-pooled-error test for identifying differentially expressed genes with a small number of replicated microarrays. *Bioinformatics* **19**, 1945–1951 (2003).